Time-resolved photon-scattering measurements from scattering media fitted to non-Euclidean and conventional diffusion models

M. E. Zevallos, A. Ya Polischuck, B. B. Das, Feng Liu, and R. R. Alfano
Institute for Ultrafast Spectroscopy and Lasers, New York State Center of Advanced Technology for Ultrafast Photonic Materials and Applications, Departments of Physics and Electrical Engineering, The City College and Graduate School of the City University of New York, New York, New York 10031
(Received 30 May 1997)

Time-resolved light scattering profiles were measured from highly forward-scattering media in the spatial range of 5–15 transport mean free paths (l_t). Experimental profiles were compared with theoretical predictions based on the non-Euclidean diffusion (NED) and conventional diffusion approximation (DA) equations. The NED model was found to be better in predicting scattered photon distribution over various temporal and spatial scales than the DA approach. [S1063-651X(98)08406-2]

PACS number(s): 42.25.Bs, 42.25.Fx, 05.60.+w

I. INTRODUCTION

Understanding photon migration in scattering media is important for its implementation in many light based imaging applications, ranging from optical tomography and mine detection, to remote sensing. The radiative transfer Boltzmann equation can describe photon migration in a random medium; however, because of its complexity several approximations have been developed, such as the diffusion approximation (DA), the telegrapher's equation [1], and higher order approximations to the Boltzmann equation [2]. These approximations with the help of fitting techniques have been used to determine the values of some key optical parameters that describe the scattering medium such as the transport mean free path (l_t) and the absorption length (l_a). The determination of these key optical parameters is important in order to predict the photon temporal distribution at a fixed point inside a scattering medium or the photon spatial evolution between two or more different points. The limitations of the DA are its inaccuracy in predicting the intensity of early arriving light and the location of the maxima intensity peak position. This inaccuracy leads to a failure in fitting experimental intensity temporal profiles obtained in the *prediffusive regime* (distances$\leqslant$5 to 7—transport mean free path—that is, 10–15 mm for human breast tissue in the near-infrared (NIR) region). The DA deficiency in predicting the nature of photon migration in a close spatial region has been shown in Refs. [3, 4]. Further improvements in this onset regime should prove useful in the detection of hidden abnormalities in medical imaging and optical tomography. It is not the distance between source (S) and detector (D) that determines the applicability of DA in optical tomography, but the distance between hidden objects (tumour) and the source (or detector). In this context, recently introduced [5,6], the non-Euclidean (NED) model in contrast to the DA offers an improvement in predicting photon transport in the prediffusive regime. Based on past experiments performed on different animal tissues the l_t is about 2.5 mm at 625 nm, and $\sim$5 mm in the NIR region [7,8]. The transport mean free path in human breast tissues is $l_t \sim 1$ mm in the visible region and is expected to be more than twice that by selecting the appropriate NIR wavelength. The S-D distances of $5l_t$ and $15l_t$ used for the measurements of this experiment correspond to typical distances between source/detectors and hidden inhomogeneities—such as tumors—located in the middle of a typical compressed human breast size of $\approx$60 mm or $30l_t$ under NIR light. Interesting tissue components in a human breast are adipose (fat), glandular, ducts, blood vessels, calcifications, and growths—each with different scattering properties.

In this paper, theoretical predictions from the NED and the DA equations obtained for the prediffusive and diffusive regions are compared with the measured scattered light temporal profiles. The NED equation represents a bridge between the ballistic regime at small l_t distances and the diffusive regime at large l_t distances. At large times, for a fixed distance the NED equation describes the diffusive regime and NED and DA approach each other.

II. NED AND DA MODELS

The photon number density function $N(t,\vec{r})$ is used to describe the temporal and spatial evolution of scattered photons originating instantaneously from a pointlike collimated source and traveling in a highly forward-scattering medium. The photon number density profiles obtained from the NED and the DA equations for an infinite medium are compared in this paper with experimental profiles in time and space.

For the DA model [9,10], the photon number density for an infinite medium is given by

$$N(t,\vec{r}) = \frac{1}{(4\pi)^{3/2}(Dt)^{3/2}}\, e^{(-1/4Dt)(\vec{r})^2} e^{-v_a t}, \qquad (1)$$

where the source is assumed at the origin and $D \approx \{c/3[(1-g)\mu_s]\} = cl_t/3$. The term $(1-g)\mu_s = \mu_s'$ is the reduced scattering coefficient; c is the speed of light, and l_t is the transport mean free path. The last exponential decay term ($e^{-v_a t}$) is the absorption term that affects the pulse profiles at large times when $t > t_a = (v_a)^{-1}$. v_a is defined as c/l_a. For this study, the absorption length in the media was fixed at $l_a = 300$ mm and the transport mean free path to $l_t = 2$ mm. The absorption dependence of D has been ne-

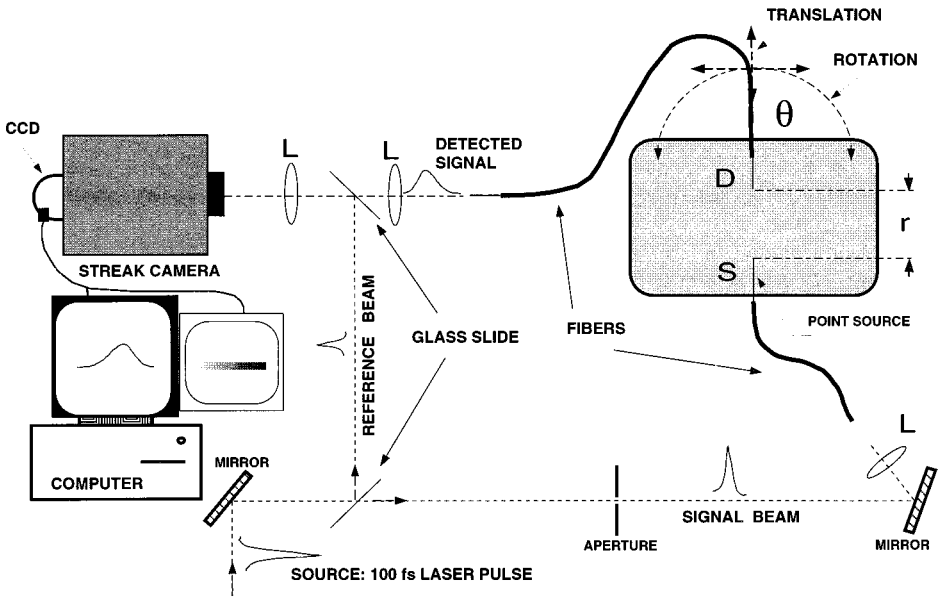

FIG. 1. Schematic diagram of the experimental setup.

glected since l_a is much larger than l_t. A problem of the absorption dependence of D was recently reconsidered in Ref. [2] and references therein.

For the NED model [5,6,11], the photon number density is given by

$$N(t,\vec{r},\vec{s}_0)=\frac{1}{(4\pi)^{3/2}}\frac{1}{\sqrt{\det\Delta}}\times\exp^{(-1/4)\Delta^{-1}_{\alpha\beta}(r-r_c)_a(r-r_c)_\beta}\exp^{-v_a t}, \quad (2)$$

where Δ is a 3×3 matrix and Δ^{-1} is its inverse. The exponential term $\Delta^{-1}_{\alpha\beta}(r-r_c)_\alpha(r-r_c)_\beta$ indicates the summation of the multiplication of the components of the inverse matrix with the components of the vector difference $(\vec{r}-\vec{r}_c)$. The components of the Δ matrix as well as the components of the vector difference are indicated by the subscripts α and β, which can take the numbers 1, 2, or 3. The components of the Δ matrix are given by

$$\Delta_{\alpha\beta}(t)=\frac{l_t^2}{2}\,\delta_{\alpha\beta}\left(\frac{2}{3}\,\tau-f_1+\frac{1}{9}\,f_3\right)+\frac{l_t^2}{2c^2}\,(s_0)_\alpha(s_0)_\beta\left(f_1-\frac{1}{3}\,f_3-f_1^2\right), \quad (3)$$

where $f_1=1-e^{-1\tau}$, $f_3=1-e^{-3\tau}$, $\tau=ct/l_t$, and $(s_0)_\alpha(s_0)_\beta$ is the multiplication of the components of the initial velocity propagation direction vector $\vec{s}_0$, which for our system is defined as $(0,0,c)$. Notice that the multiplication $(s_0)_\alpha(s_0)_\beta$ will only survive for α and β equal to 3 for our particular experimental system, i.e., light propagation in the z direction. On the other hand, $(r-r_c)_\alpha(r-r_c)_\beta$ indicates the multiplication of components of the vector difference $(\vec{r}-\vec{r}_c)$. Here, $\vec{r}$ is the detector location or final photon trajectory detection position; $\vec{r}_c(t)$ is the position of the center of mass of the photon cloud and it is equal to $\vec{r}_c(t)=\langle\vec{r}(t)\rangle=\vec{s}_0(l_t/c)(1-e^{(ct/l_t)})$. The symbol $\langle\cdots\rangle$ stands for the averaging over all trajectories with the same initial velocity propagation $\vec{s}_0$.

From Eq. (2) for small times $t\ll(l/c)$ one has $\Delta_{\alpha\beta}\to0$ and $N(t,\vec{r},\vec{s}_0)\to\delta(\vec{r}-\vec{s}_0t)$; the ballistic regime is recovered. On the other hand, for larger times $t\gg(l_t/c)$, $\Delta_{\alpha\beta}\to\delta_{\alpha\beta}(cl_tt/3)=Dt$; the diffusion regime is attained and the solution for the NED equation $N(t,\vec{r},\vec{s}_0)$ approaches to the solution of the conventional DA. Note that the photon number density in Eqs. (1) and (2) is normalized to the initial number of photons in the pulse.

The time-resolved intensity profile from red scattered light was measured in the range 10–30 mm (5 to $15l_t$) for a calculated $l_t=2$ mm value to check on the predictions of the NED-based [Eq. (2)] and the conventional DA [Eq. (1)]. It should be noted that even at distances as large as $15l_t$ the photon number density predicted by the NED and by the conventional DA differ appreciably [5].

III. EXPERIMENTAL METHOD

The schematic diagram of the experimental setup is shown in Fig. 1. A laser of ultrashort pulses of 100 fs duration at 82 MHz pulse repetition rate and 10 mW with average power generated from a colliding-pulse mode-locked (CPM) dye-laser system was used to simulate an instantaneous point source. The wavelength of laser pulses was centered at 625 nm. The laser beam was split into a reference and signal beam by a glass slide. The reference beam was used to mark the zero time of the signal beam and to monitor the intensity fluctuations of the laser. The signal beam was coupled into the medium using a 100-mm focal length lens and an optical fiber. A 10-ps resolution streak camera was used to measure the collected scattered pulse traveling inside the highly scattering medium.

The scattering media consisted of polystyrene microspheres and absorbing dye suspended in deionized water. The diameter of the polystyrene spheres was 1.11 μm. A

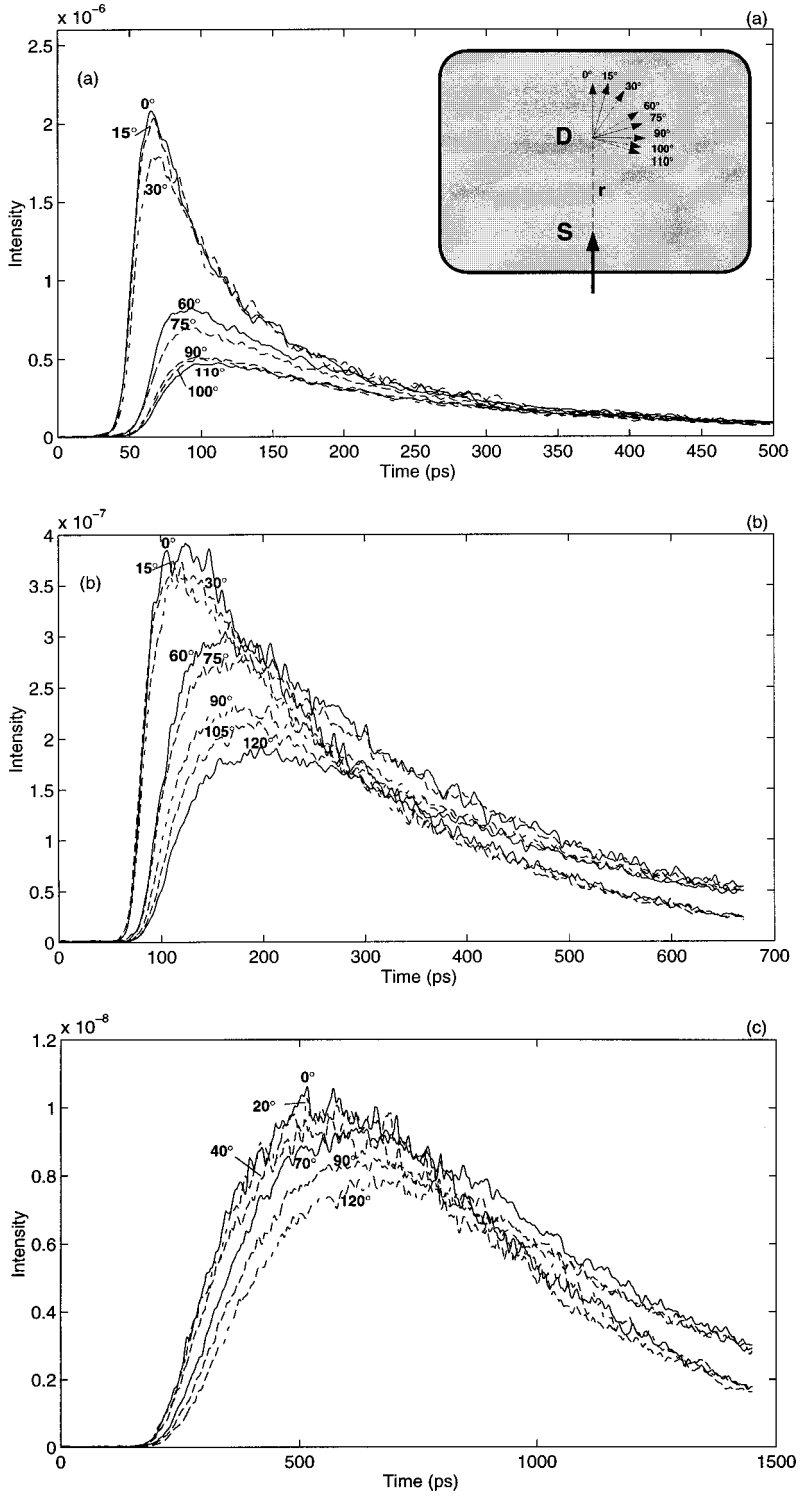

FIG. 2. Scattered light intensity temporal profiles measured at various distances for different detection angles. The medium optical parameters are $l_t = 2.00 \pm 0.04$ mm and $l_a = 300$ mm. The inset shows a schematic of the source and detector angular positions. The point of detection was situated along the pulse launching direction. The plots in (a)–(c) show the measurements obtained at distances $r = 5$, 7, and $15 l_t$, respectively, for various detection angles.

scattering concentration (of polystyrene sphere) of 0.169% of the total volume was selected to ensure $l_t = 2.00 \pm 0.04$ mm. The absorption length was set to $l_a = 300$ mm by adding a calculated small amount of absorbing dye (Malachite Green) to the scattering medium. The scattering mean free path (l_s) and scattering mean cosine factor (g) were 0.144 and 0.926, respectively. The value of l_t was calculated on the basis of the Mie theory. For such a concentration of scattering particles l_t was experimentally shown to be proportional to the number density of scatters [12]. The scattering medium was placed in a transparent cylindrical tank of 100 mm in diameter and 100 mm in altitude.

To simulate a point source and a point detection, the signal light was guided into and out of the medium by means of

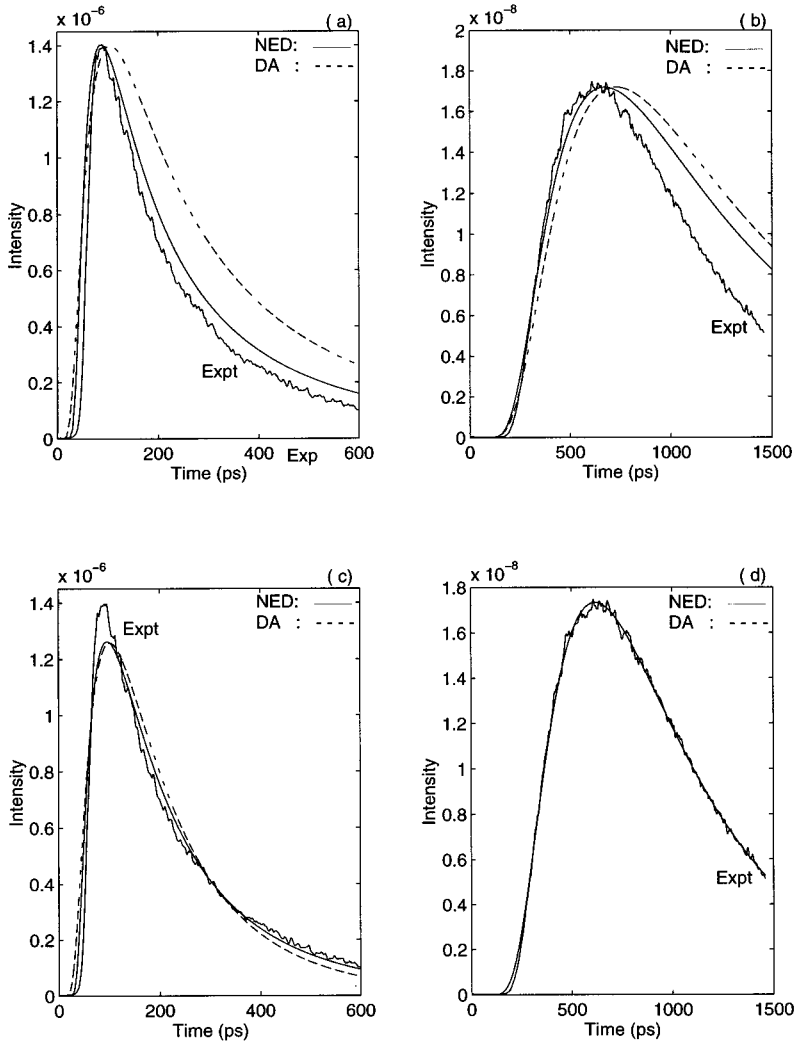

FIG. 3. Angle averaged scattered light intensity temporal profiles measured and calculated using the NED and DA at $r=5$ and $15l_t$. In (a) and (b), the theoretical intensity temporal profiles for both models are calculated using the *a priori* known optical parameters $l_t=2.00$ mm and $l_a=300$ mm for distances 5 and $15l_t$, respectively. In (c) and (d) for the same distances the theoretical profiles use the best fit optical parameters calculated in Table I using the best fit approach.

two 200-μm core diameter optical fibers with a numerical aperture (N.A.) inside the medium of 0.287. These fibers represented the S and D. The input fiber (S) was fixed at one of the walls of the tank. The D was mounted on a x-y-z translational and angular (θ) rotational stage and positioned on the optical axis right across the source direction ($\vec{s}_0$). The translational stage was used to vary the source-detector distance r while the angular rotational stage was used to rotate the detector and collect the light arriving from different directions at a fixed point. The output of the detection fiber (scattered signal) was focused into the input slit of the streak camera.

Intensity temporal profiles $I(t,r,\vec{m},\vec{s}_0)$ were measured at various distances r and various angular orientations $\vec{m}$, where $\vec{m}$ is the orientation of the detecting fiber with respect to the propagation direction $\vec{s}_0$ [see inset in Fig. 2(a)].

The measured intensities are related to the photon specific number density $n(t,\vec{r},\vec{s},\vec{s}_0)$ by

$$I(t,r,\vec{m},\vec{s}_0)=\int d\vec{s}\,A(\vec{m},\vec{s})n(t,\vec{r},\vec{s},\vec{s}_0), \tag{4}$$

where $A(\vec{m},\vec{s})d\vec{s}$ is the ratio of the number of photons in a solid angle $d\vec{s}$ collected by the detector per unit time to the photon flux in the $\vec{s}$ direction. For additional information on the receiving cross sectional area for the receiver see Refs. [13–16].

The *angular-integrated intensity temporal profile* $I(t,\vec{r},\vec{s}_0)$ is represented as [11] by

$$I(t,r,\vec{s}_0)=\int d\vec{m}\,I(t,r,\vec{m},\vec{s}_0)=WN(t,\vec{r},\vec{s}_0), \tag{5}$$

where $W=\tilde{A}cN_0$; N_0 is the number of photons in the incident pulse, and $\tilde{A}=\int d\vec{m}A(\vec{m},\vec{s})$ is a constant characterizing the effective fiber system receiving area.

The corresponding experimental temporal profiles detected with different angles of collection $\vec{m}$ at a fixed spatial point r were combined to obtain an *angular-integrated intensity temporal profile* $I(t,\vec{r},\vec{s}_0)$. The procedure described above makes possible the comparison of the experimental angular-integrated intensity temporal profiles for a fixed dis-

tance r (presented in Fig. 2) with the theoretical result *predicted* by the NED and DA equations.

IV. EXPERIMENTAL RESULTS

In this experiment, the source-detector distance was varied from $5l_t$ to $15l_t$; at each distance r, scattered pulse profiles $I(t,r,\vec{m},\vec{s}_0)$ of various angular orientations were measured. Figs. 2(a)–2(c) show intensity temporal profiles obtained for $r=5$, 7.5, and $15l_t$ respectively. Each temporal profile in Fig. 2 has been labeled with its respective angle of detection ($\vec{m}$). The inset in Fig. 2(a) shows a schematic of the source and detector position and angular orientations for a fixed distance r. These profiles were averaged to obtain $I(t,\vec{r},\vec{s}_0)$.

The salient features of profiles shown on Fig. 2(a) for $5l_t$ are the following. (a) The highest-intensity temporal profiles for a point in space are localized along the launching direction and around the 0° detector angular orientation. (b) As the angle of rotation is increased away from the 0° collinear direction, the temporal profiles are affected and the following features are observed: (i) the intensity temporal profile decreases; (ii) the early light (snake light) and the time to reach the intensity peak (T_p) is delayed in time; (iii) there is an increased in the full width at half-maximum (FWHM) and the scattered pulse becomes broadened. These features were consistent for all distances in the range chosen for this study ($5l_t$ to $15l_t$) and can also be observed in Figs. 2(b) and 2(c). The strong angular and spatial dependence of photons traveling in a highly scattering medium in the forward direction (source launching direction) and lateral direction (perpendicular to source launching direction) have previously been mentioned in Ref. [17]. In this work only light propagation in the forward direction was considered. In the near zone at a fixed distance r, the local scattered light intensity is strongly angular dependent. This local angular dependence (anisotropy) gradually decreases with time as a result of multiple scattering. For a *fixed point*, photon distribution in time becomes more isotropic as time passes; in addition, the intensity detected at a fixed point decays as we move away from the source. When comparing profile groups obtained at different distances, another important feature can also be observed: mainly, the striking difference due to the angle of detection dependence starts fading away as the source-detector distance is increased. It is clear that even at the distance $15l_t$ the angular distribution of light is still appreciably anisotropic. Note that almost isotropic angular distribution of photons is a necessary condition for the diffusion model to be valid.

V. DISCUSSION

The curves in Figs. 3(a) and 3(b) show the experimental angular-integrated intensity temporal profiles $I(t,\vec{r},\vec{s}_0)$ for $r=5$ and $15l_t$ together with the *normalized* photon number density temporal profiles calculated using the NED and the ordinary diffusion approximation DA. The theoretical curves calculated for different distances r were normalized to the experimental peak intensity values obtained at each distance, respectively. The *a priori* known optical parameters l_t and l_a used in the prediction of these theoretical curves were 2 and

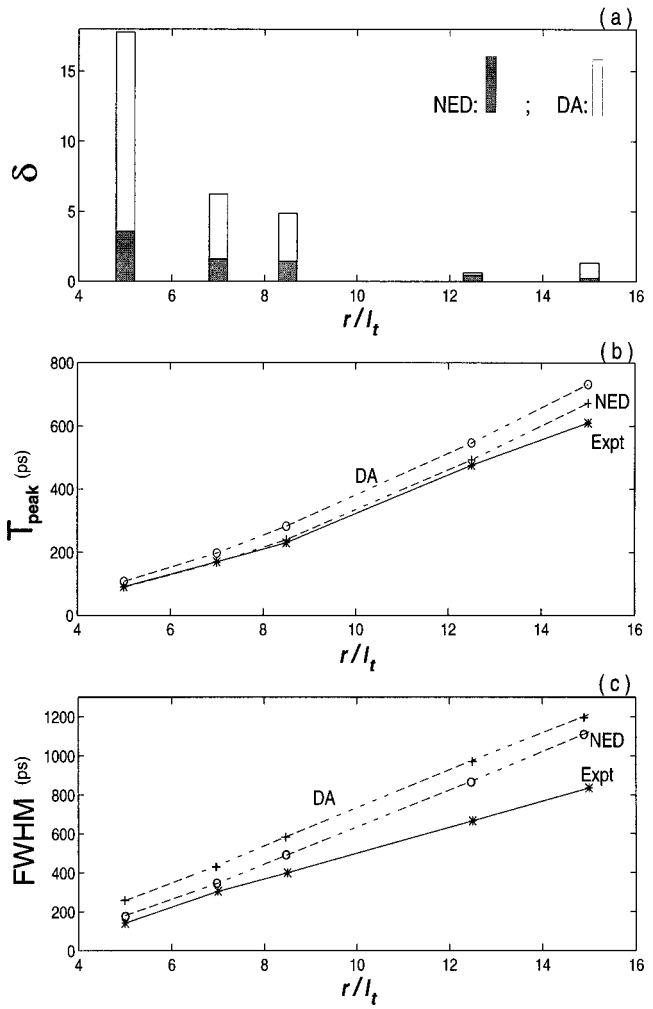

FIG. 4. General properties of scattered intensity temporal profiles predictions. (a) Relative deviation δ (see text) of theoretical curves from an experimental intensity temporal profiles for the NED (open rectangles) and DA (filled rectangles) at various distances from the source; (b) FWHM for the calculated and measured temporal profiles; and (c) temporal position of the peak of the scattered light intensity vs source-detector distance.

300 mm, respectively. The curves predicted by the DA have been plotted using dashed lines, while the NED predictions use a smooth solid line. The difference in *shape accuracy* of the theoretical curves with respect to the experimental data is presented in Fig. 4(a). Although theoretical curves were normalized to experimental data, NED and DA predictions (profiles) still showed considerable differences for different distances, as is shown in Figs. 3(a) and 3(b). The experimental data favors more the curves predicted by the NED theory than the ones predicted by the DA. It should be emphasized once again that the theoretical curves plotted in Figs. 3(a) and 3(b) *do not use the best fitting parameter* approach; instead, we make use of the *a priori* known actual parameters (e.g., $l_t=2$ and $l_a=300$ mm) of the scattering medium to plot both theoretical curves.

Since the theoretical results were obtained for an infinite medium while the experiment was performed in a finite medium (e.g., a tank 100 mm in diameter), an estimated time (T_m) where the walls of the tank commence to affect the experimental measurements was found to start at around 600

TABLE I. Best fitting values (l_t, l_a) to the measured temporal profiles for NED and DA for different distances r.

Distance	Ned best fitting parameters		DA best fitting parameters	
r (mm)	l_t (mm)	l_a (mm)	l_t (mm)	l_a (mm)
10	1.69	101.6	1.75	62.24
14	1.64	104.0	1.73	82.4
17	1.66	102.1	1.74	85.4
25	1.68	125.0	1.77	115.3
30	1.81	145.3	1.91	137.4

ps. We attribute the intensity mismatch of the experimental temporal profile with respect to the theoretical curves shown at the falling wing in Fig. 3(b) to the *boundary effects* (for $t > T_m$) since photons escaping through walls are equivalent to surface absorption. Therefore the region between 0 and 600 ps should be considered for the match with theory.

The fitting of the key parameters l_t and l_a of the experimental data obtained by both theories for different distances is displayed in Table I. The values in Table I correspond to the best fitting predicted by both theories while using the *least square curve fitting* technique.

The best fitting parameter values from Table I are used to plot the theoretical intensity temporal profiles for the NED and the DA models for distances $r=10$ and $r=30$ mm and are compared to the experimental data in Figs. 3(c) and 3(d), respectively. The average value found through the best fitting approach for l_t and l_a is 1.7 and 115.6 for the NED and for the DA, 1.78 and 96.54, respectively.

Although the values obtained through fitting differ from the *a priori* known fixed values $l_t=2$ and $l_a=300$ mm, both theories could provide a good fit. Notice that, although fitted, l_a shows an strong dependence on distance especially for the DA. Table I indicates that the simple two parameter fitting procedure may not be a correct way to obtain the l_t and l_a parameters since the values obtained differ significantly, given errors over 13% and 100% for l_t and l_a, respectively.

The relative error, deviation δ of normalized predicted theoretical curves $I_T(t)$ from experimental intensity temporal profiles $I_{\text{expt}}(t)$, was calculated for different distances r in order to have a feeling of the *shape accuracy* for both theories. The relative deviation was characterized by a parameter $\delta = 100\|I_T(t) - I_{\text{expt}}(t)\|/\|I_{\text{expt}}(t)\|$ where $\|I(t)\| = \sqrt{\int_0^{T_m} I^2(t)dt}$ is the L_2 norm of the Intensity function $I(t)$ defined on a segment $[0,T_m]$. Figure 4(a) shows a histogram plot of the relative deviation δ of both models using $l_t=2$ and $l_a=300$ mm. To avoid the boundary effects, the parameter δ was calculated using the first 600 ps of the experimental and theoretical profiles for distances r/l_t of 5, 7, 8.5, 12, and 15. It can be observed in this histogram that the relative deviation δ is bigger for the DA than for the NED mainly in the close region 5, 7, and $8.5 l_t$. These results demonstrate that the NED describes the shape of the intensity temporal profiles of scattered light better than the DA does at different spatial positions.

The plot of the FWHM of the experimental and theoretical temporal profiles is shown in Fig. 4(b) for each distance (r/l_t). A large deviation arising from the boundary effects is observed in the FWHM for distances $r/l_t = 12.5$ and 15. The theoretical FWHM values predicted by the NED model were found to be closer to the experimental results than those predicted by the DA.

The plot in Fig. 4(c) shows the T_p corresponding to the maxima intensity temporal position for different distances r

TABLE II. Best fitting values (l_t') and respective errors (e) for NED and DA obtained by keeping fixed the *a priori* known parameter $l_a=300$ mm fixed for different distances r; best fitting values (l_a') and respective errors (e) for NED and DA obtained by keeping fixed the *a priori* known parameter $l_t=2$ mm fixed for different distances r.

Distance	NED best l_t' fitting parameter			DA best l_t' fitting parameter		
r (mm)	fixed l_t' (mm)	l_a (mm)	$e=100\left\|\frac{2-l_t'}{2}\right\|$	fixed l_t' (mm)	l_a (mm)	$e=100\left\|\frac{2-l_t'}{2}\right\|$
10	1.96	300	2.0%	2.49	300	**24.5%**
14	1.93	300	3.5%	2.25	300	12.5%
17	1.99	300	**0.5%**	2.26	300	13.0%
25	1.91	300	**4.5%**	2.08	300	**4.0%**
30	1.98	300	1.0%	2.12	300	6.0%

Distance	NED best l_a' fitting parameter			DA best l_a' fitting parameter		
r (mm)	fixed l_t (mm)	l_a' (mm)	$e=100\left\|\frac{300-l_a'}{300}\right\|$	fixed l_t (mm)	l_a' (mm)	$e=100\left\|\frac{300-l_a'}{300}\right\|$
10	2.0	223.8	25.4%	2.0	80.0	**73.3%**
14	2.0	252.5	15.8%	2.0	119.0	60.3%
17	2.0	223.0	25.6%	2.0	122.0	59.3%
25	2.0	392.0	**30.6%**	2.0	190.2	**36.6%**
30	2.0	281.8	**6.0%**	2.0	167.7	44.1%

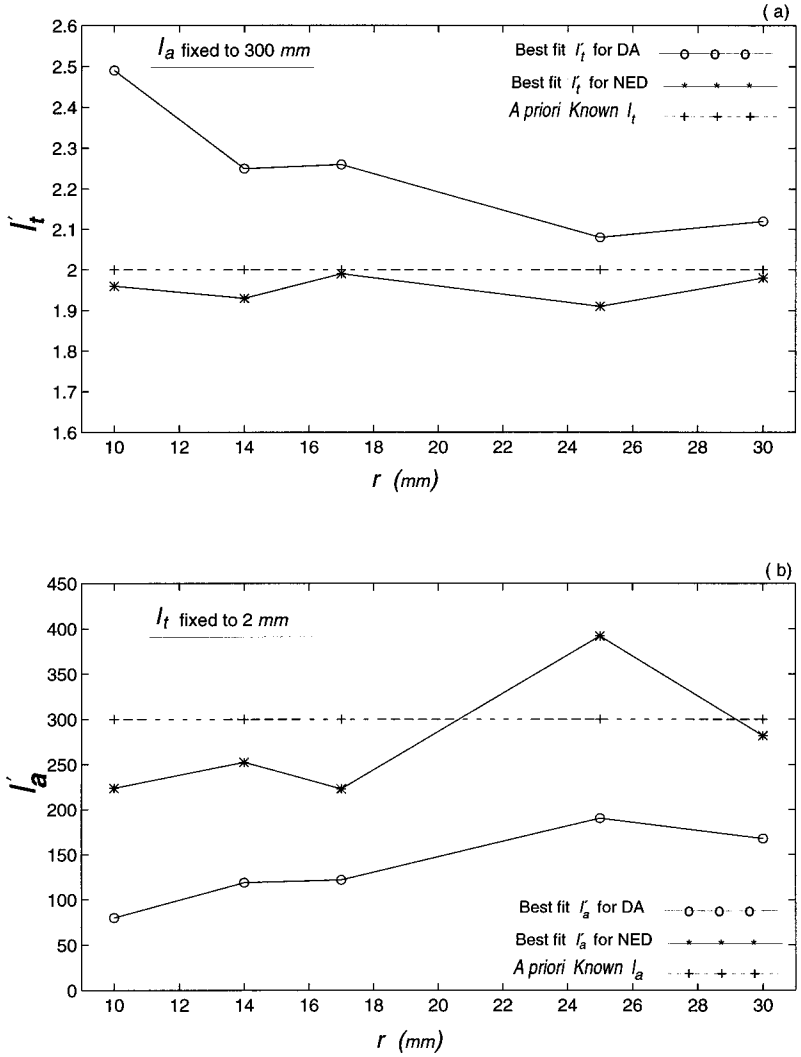

FIG. 5. Best fit optical parameters retrieved from the scattered light intensity measurements at different distances using the NED and DA theories. The dashed line represents *a priori* known values $l_t = 2.00$ mm and $l_a = 300$ mm. See text for more details. (a) *A priori* known value l_a is kept fixed to 300 mm while obtaining l'_t best fits; (b) *a priori* known value l_t is kept fixed at 2 mm while obtaining l'_a best fits.

for both models NED and DA, and for the experimental results. It could be observed that the T_p values for the DA model are further apart from the experimental values than the ones obtained by the NED model. This time peak shift in the DA profiles has been observed before and addressed in Refs. [3, 4]. *The main advantage of the NED versus the DA model is that the NED model can describe with greater accuracy the transition between ballistic and developed diffusion regimes, e.g., that it is where the DA starts to fail.*

To determine the accuracy of both models when only one parameter l_a or l_t is known in advance, the standard best fitting approach has been used to calculate one of these optical parameters while the other one has been kept fixed. The results are given in Table II. The parameters l'_t obtained as a result of fitting the NED and DA to the experimental data taken at different distances from the source (r) holding the *a priori* known value of l_a fixed (e.g., equal to 300 mm) are plotted in Fig. 5(a). This figure shows the variation of the fitted value l'_t with respect to *a priori* calculated l_t value (e.g., equal to 2 mm) given by the NED and the DA theory for different distances. The fitted l'_t values predicted by the NED and DA are plotted using stars ($\star$) and circles ($\bigcirc$), respectively, and are connected with solid lines, while the *a priori* l_t constant known values have been plotted using plus signs ($+$) and are connected by dashed lines. The mean transport length values predicted by the DA show a higher deviation than those predicted by the NED. The variation of error (e) to the fitted parameter l'_t with respect to $l_t = 2$ mm has also been tabulated in Table II and ranges from 0.5% to 4.5% for the NED model and from 4.0% to 24.5% for the DA model. In a similar manner, the best fit is shown for l'_a obtained by both models for different distances while keeping fixed the *a priori* calculated l_t value equal to 2 mm. The error given by fitting the absorption length l'_a with respect to $l_a = 300$ mm has been tabulated in Table II. Figure 5(b) depicts the results of Table II. Once again the predicted l'_a values obtained by the NED and DA are plotted using stars ($\star$) and circles ($\bigcirc$), respectively, and are connected with solid lines, while the *a priori* l_a constant known value has been plotted using plus signs ($+$) and are connected by dash lines. Notice that *the margin of error* for l'_a is *below 30.6%* for the NED and *above 36.6%* for the DA model with respect to the *a priori* fixed and constant known value $l_a = 300$ mm.

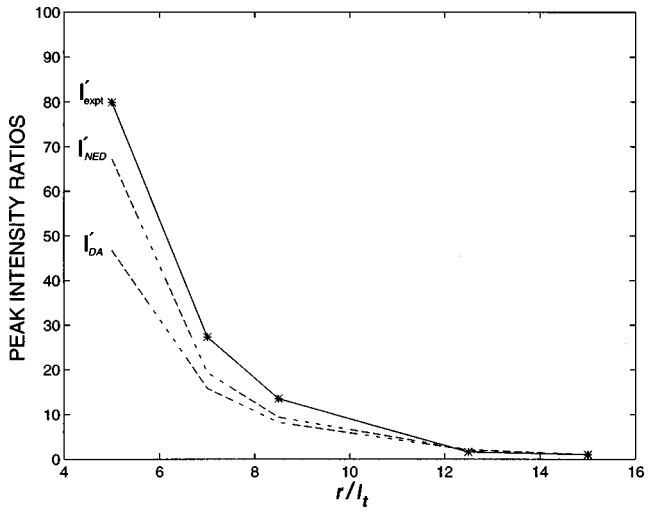

FIG. 6. Relative peak intensity ratios vs source-detector distance. Peak intensity values were obtained from experimental and theoretical profiles at the peak time (T_p). The peak intensity ratio was taken for different distances r with respect to the individual peak intensity values obtained experimentally and theoretically at $r=15l_t$ as follows: $I'_{\text{expt}}=I_{\text{expt}}(r,T_p)/I_{\text{expt}}(15l_t,T_p)$, $I'_{\text{DA}}=I_{\text{DA}}(r,T_p)/I_{\text{DA}}(15l_t,T_p)$, and $I'_{\text{NED}}=I_{\text{NED}}(r,T_p)/I_{\text{NED}}(15l_t,T_p)$.

Figures 5(a) and 5(b) show that, when a parameter l_t or l_a is *a priori* known, the NED model will predict with a considerably higher accuracy the unknown parameter values (l'_a or l'_t) than the DA at any distance in the prediffuse regime.

In Figs. 3 and 4, we have compared to the experimental data only the *shape* of the *normalized theoretical curves* predicted by both models, which correspond to the *photon temporal distribution at fixed distances*. To make a fair comparison between the two theories and the experiment, one needs to observe not only the prediction of *the temporal evolution of local photons (i.e. distribution of photons in time at a fixed distance r)* but also the consistency in predicting *the spatial-temporal distribution of scattered light at different distances*. On the other hand, an absolute direct comparison of the intensities calculated and measured at different spatial locations is difficult since the effective receiving cross section $\tilde{A}$ in Eq. (3) and the number N_0 of the initially launched photons have not been measured in the experiment (see also the respective discussion below). A relative comparison at different distances r does provide critical information regarding the capabilities of the NED and DA in describing *the scattered light distribution in space and time*. Intensity peak ratios $I_{\text{peak}}(r,T_p)/I_{\text{peak}}(15l_t,T_p)$ obtained from the experimental profiles and both theories have been plotted in Fig. 6 for different distances r. The experimental values in Fig. 6 are

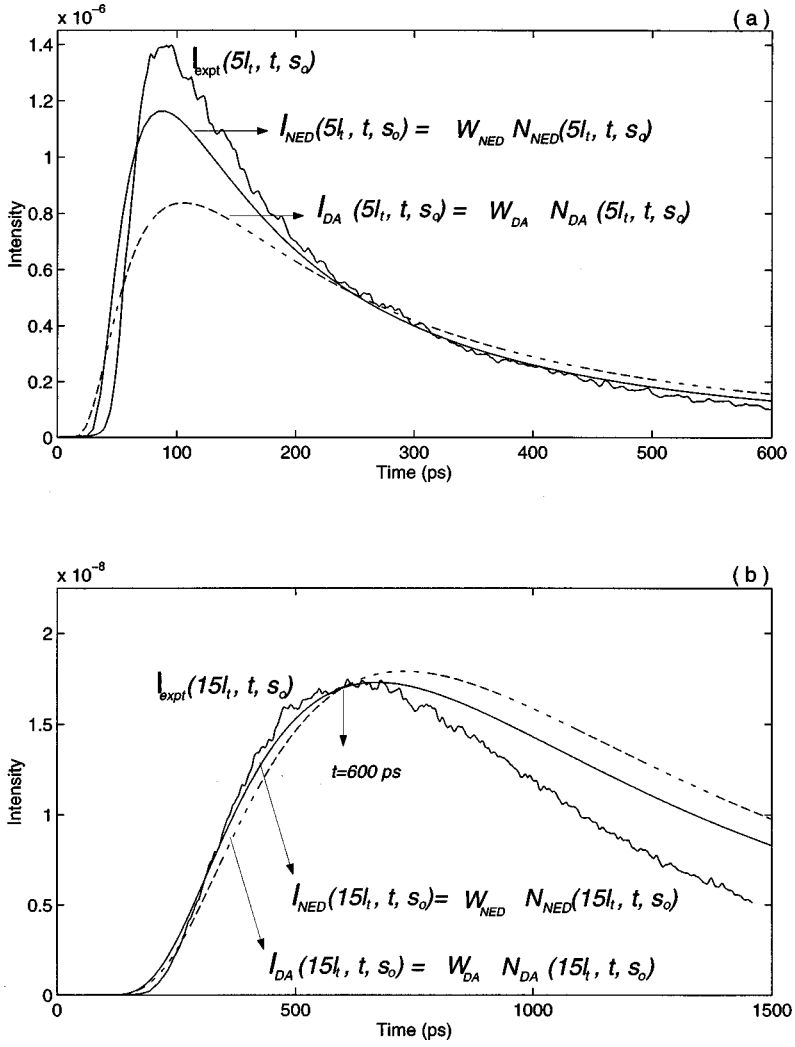

FIG. 7. Experimental scattered light intensity temporal profiles and theoretical profiles calculated using the NED and DA after the introduction of individual normalization factors W_{NED} and W_{DA} obtained at $r=15l_t$ and at $t=600$ ps. See text for more details. The medium parameters are $l_t=2.00\pm0.04$ mm and $l_a=300$ mm. Plots in (a) and (b) were measured and calculated at $r=5$ and at $15l_t$, respectively.

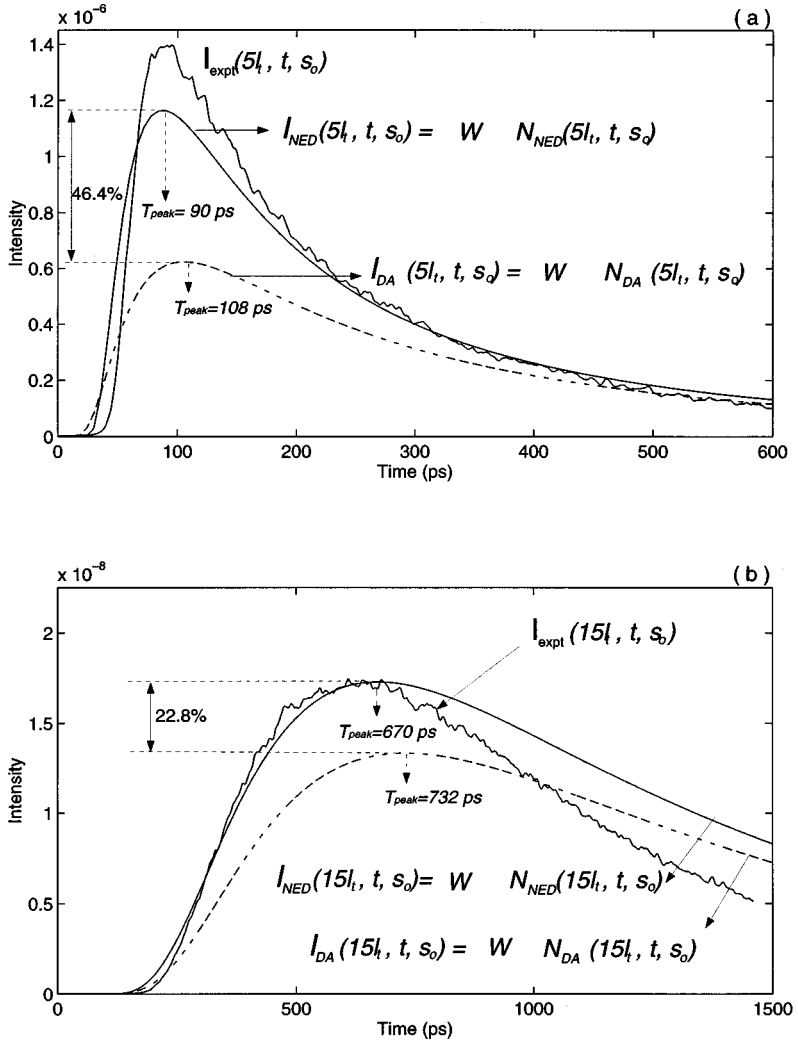

FIG. 8. Direct comparison of both models using a common weight factor $W=0.0405$. The medium parameters are $l_t=2.00\pm0.04$ mm and $l_a=300$ mm. Plots in (a) and (b) were measured and calculated at $r=5$ and $15l_t$, respectively.

connected with a solid line while the ones obtained by both theories are connected with dashed and smooth solid lines. The intensity ratios in Fig. 6 provide insight into the consistency and accuracy of both theories in predicting intensity values at different spatial locations. Looking at the intensity ratios predicted by both theories, one could observe a larger deviation for the DA with respect to the experimental values in the close region (below $10l_t$) as expected. This figure mainly demonstrates that the spatial distribution of scattered light intensity is better described by the NED than by the DA.

A similar comparison could be done by using the absolute intensity values predicted by each theory. In order to do this, one needs to use directly the experimental intensity values $I_{\text{expt}}(t,\vec{r},\vec{s}_0)$ and compare them independently to the intensity values predicted by both theories $[I_{\text{NED}}(t,\vec{r},\vec{s}_0),\ I_{\text{DA}}(t,\vec{r})]$, *in time and space*. Although the parameters $\tilde{A}$ and N_0 are *a priori* unknown, we may use fitting of either theories to the experimental data to determine an intensity normalization factor $W=\tilde{A}cN_0$. Since the photon number density values of both theories differ from each other the factor W will be individual for each theory; however, for a consistent theory W should be the same when comparing theoretical and experimental intensities at different times and distances. Since the NED and DA models approach each other at large l_t distances and at large times, we have picked W from the experimental intensity temporal profile at $r=15l_t$ (the furthest distance in our experiment) and at $t=600$ ps (later times are strongly subject to our boundaries constraints). We calculate W for each theory as follows: for the NED theory $W_{\text{NED}}=I_{\text{expt}}(t=600,\vec{r}=30,\vec{s}_0)/N_{\text{NED}}(t=600,\vec{r}=30,\vec{s}_0)$, and for the DA theory $W_{\text{DA}}=I_{\text{expt}}(t=600,\vec{r}=30,\vec{s}_0)/N_{\text{DA}}(t=600,\vec{r}=30)$. The values found for W_{NED} and W_{DA} were 0.0405 and 0.0545, respectively.

The plots in Figs. 7(a) and 7(b) show the experimental profiles obtained at $r=10$ and 30 mm (e.g., 5 and $15l_t$) compared with two theoretical curves—$I_{\text{NED}}(t,\vec{r},\vec{s}_0)=W_{\text{NED}}N_{\text{NED}}(t,\vec{r},\vec{s}_0)$ and $I_{\text{DA}}(t,\vec{r})=W_{\text{DA}}N_{\text{DA}}(t,\vec{r})$—obtained after the introduction of the intensity weight factors W_{NED} and W_{DA} at $t=600$ ps and $r=30$ mm. In these figures, the *a priori* known values $l_t=2$ and $l_a=300$ mm have been used. At $t=600$ ps, an exact matching in intensities for both theories and experiment is observed in Fig. 7(b). This matching is a result of the individual intensity factors (W_{NED} and W_{DA}) introduced by each theory. In the same plot [Fig. 7(b)] for $t<600$, the intensity values at different times

for the NED model are in better agreement with the experimental intensity values than those for the DA model. This asymptotic intensity matching should be consistent at shorter distances. Indeed, the NED is shown to be in better agreement to the experimental intensity values than the DA at these distances—see Fig. 7(a). The agreement of the intensities predicted in the prediffusive regime by the NED at different time and at different spatial positions is shown to be more consistent than intensity values predicted by the DA. In fact, intensity peak values predicted by DA at short distances ($r \leqslant 10 l_t$) are underestimated by about 40% with respect to the experimental values. It should also be mentioned that choosing a bigger W_{DA} value (in order to have a better intensity match at $5 l_t$) will overestimate the intensity values obtained at $15 l_t$ and beyond. The factor obtained by W_{NED} is considered to be a more reliable value since it is shown to be more consistent with the experimental results at different times and distances as shown in Figs. 7(a) and 7(b). In order to have a direct comparison of both theories and experimental results, we have plotted in Figs. 8(a) and 8(b) the intensity predicted by each theory using a common factor ($W = W_{\mathrm{NED}}$) as well as the profiles obtained experimentally for distances $5 l_t$ and $15 l_t$, respectively. Performing a direct comparison of the two theories under a common factor W clearly shows appreciable intensity differences between them. These differences are observed in the peak intensity values as well as in time peak positions (T_{peak}). Figure 8(a) shows a 46.4% peak intensity difference between the two theories plus a delay in time of 18 ps for the DA. Figure 8(b) shows a 22.88% peak intensity difference between the two theories and a delay in time of 60 ps for the DA. The intensity difference of the two theories decreased for large lt distances as expected since the NED model takes the form of the DA. Also in Fig. 8, the DA model can be compared to the experimental results. Here a complete intensity mismatch of the DA could be observed with respect to the experimental results at different times and distances. Asymptotic comparison of intensities in time of the two theories for different distances (spatial locations) with respect to experimental values is essential and provides a better description of the capabilities of both theories. *The NED model in contrast to the DA showed a satisfactory and consistent description of scattered light intensity at most distances and times.*

In conclusion, we have demonstrated by a comparative study that the NED model provides a better description of the temporal and spatial evolution of scattered light than the DA does without taking boundary conditions into account. Appreciable differences between the NED and DA were observed for photon number density for distances as large as 10 to $15 l_t$. Even larger differences are expected for specific number density. The NED approach may be considered as a possible alternative to the DA in future optical imaging algorithms. It is worth mentioning here that the good agreement with the experimental data reported in this paper by the NED in the prediffusive regime (short range) makes it a good candidate to become a mathematical basis for the nonstationary LIDAR equation.

This work was supported in part by ONR, NASA IRA and the New York State Science and Technology Foundation.

[1] P. M. Morse and H. Feshbach, *Methods of Theoretical Physics* (McGraw-Hill, New York, 1953), Part 1, p. 865.

[2] A. Ya. Polishchuk, S. Gutman, M. Lax, and R. R. Alfano, J. Opt. Soc. Am. A **14**, 230 (1997).

[3] K. M. Yoo, Feng Liu, and R. R. Alfano, Phys. Rev. Lett. **64**, 2647 (1990).

[4] K. M. Yoo, Feng Liu, and R. R. Alfano, Proc. SPIE **1204**, 492 (1990).

[5] A. Ya. Polishchuk and R. R. Alfano, Opt. Lett. **21**, 916 (1996).

[6] A. Ya. Polishchuk, M. E. Zevallos, F. Liu, and R. R. Alfano, Phys. Rev. E **53**, 5523 (1996).

[7] K. M. Yoo, B. B. Das, F. Liu, and R. R. Alfano, Proc. SPIE **IS11**, 425 (1993).

[8] Feng Liu, K. M. Yoo, and R. R. Alfano, in *OSA Proceedings on Advances in Optical Imaging and Photon Migration*, edited by R. Alfano (OSA, Washington, D.C., 1994), Vol. 21, p. 170.

[9] Samuel Glasstone and Milton C. Edlund, *The Elements of Nuclear Reactor Theory* (Van Nostrand, New York, 1952), pp. 174–180.

[10] *Nuclear Physics*, edited by Jay Orear, A. H. Rosenfeld, and R. A. Schluter (University of Chicago Press, Chicago, 1950), pp. 187–189.

[11] A. Ya Polishchuk (unpublished).

[12] G. H. Watson, S. L. McCall, P. A. Fleury, and K. B. Lyons, Phys. Rev. B **41**, 10 947 (1990).

[13] A. Ishimaru, *Wave Propagation and Scattering in Random Media* (Academic, New York, 1978).

[14] John Gowar, *Optical Communication Systems*, 2nd ed. (Prentice Hall, New York, 1994), pp. 34–36 and 337–338.

[15] Leo Levi, *Applied Optics* (Wiley, New York, 1996), Vol. 2, pp. 231–233.

[16] John R. Taylor, *Scattering Theory: The Quantum Theory of Nonrelativistic Collisions* (Wiley, New York, 1972), pp. 44–51.

[17] M. E. Zevallos, F. Liu, B. B. Das, A. Ya Polischuck, and R. R. Alfano, in *OSA Trends in Optics and Photonics on Advances in Optical Imaging and Photon Migration*, edited by R. R. Alfano and James G. Fujimoto (OSA, Washington, D.C., 1996), Vol. II, pp. 21–24.